Leaf extract of *Cimbopogan citratus* supported CuO/ZnO nanocomposite and their applications in photocatalytic and antibacterial activities

Igneshgrace A. and Sindhuja E.*
PG and Research Department of Chemistry, Sri Paramakalyani College, Alwarkurichi, Affiliated to Manonmaniam Sundaranar University, Abishekapatti, Tirunelveli, Tamil Nadu, INDIA
*sindhujaelangovan@gmail.com

Abstract

We have focused on the green synthesis of copper oxide nanoparticles (CuONPs) and zinc oxide nanoparticles (ZnONPs) and CuO coated with ZnO nanocomposite (CuO/ZnO) by using leaf extract of Cimpobogan citrates (CC) as reducing and stabilizing agent. Copper sulfate pentahydrate ($CuSO_4.5H_2O$) and zinc acetate dihydrate ($Zn(CH_3COO)_2.2H_2O$) are the forerunners in the hydrothermal synthesis. The prepared ZnONPs, CuONPs and CuO/ZnO nanocomposite were characterized using various instrument techniques such as Fourier Transform-Infrared spectroscopy (FT-IR), UV-visible spectroscopy (UV-Vis), X-ray diffraction pattern (XRD), Scanning electron microscope (SEM), Energy dispersive X-ray analysis (EDAX) and High Resolution-Transmission Electron microscope (HR-TEM). The results showed that the average size of CuO/ZnO nanocomposite was 20-50 nm. The Tauc plot of CuO/ZnO nanocomposite shows low band gap (1.56ev). Under visible light illumination, methylene blue (MB) was degraded photocatalytically using ZnONPs, CuONPs and CuO/ZnO nanocomposite which was then examined using UV-visible spectroscopy.

In comparison to ZnONPs (65%) and CuONPs (80%), CuO/ZnO nanocomposite showed superior photocatalytic activity for the breakdown of MB with a high percentage degradation efficiency (85%). The photocatalytic degradation rate constant was evaluated by using a pseudo-first order kinetic equation. Additionally, the agar disc diffusion method was used to examine the antibacterial activity against two bacterial strains (Escherichia coli and Staphylococcus aureus) and a sizable zone of inhibition against the bacterial strains was found.

Keywords: *Cimbopogan citratus* (CC), CuO/ZnO nanocomposite, Photocatalytic degradation, Visible light irradiation, Methylene blue, Antibacterial studies.

Introduction

The goal of the current nanotechnology is to create nanoparticles using environment friendly methods with unique properties[22,25,27] that can be employed in a variety of industries. Metal oxide nanocomposites are increasingly being used for water pollution treatment, fuel cells, sensors, antibacterials and UV protection due to their sustainable development characteristics, lack of secondary pollution and high photocatalytic degradation efficiency[16,47,51]. Recently, metal oxide nanocomposites such as CuO-ZnO[7], CeO_2-MnO_x[20], ZnO-MgO[48], MgO-CuO[17], TiO_2-WO_3[8], Dy_2O_3-CuO[24], CeO_2-ZnO[13] and Co_3O_4-ZnO[12,38] which act as semiconductors, have been synthesized. Since they exhibit tunable band gap, they can be exploited as photocatalyst for degaradation of dyes.

Zinc oxide (ZnO), an n-type semiconductor, has some appealing green features such as cheap cost, great stability, non toxicity, favorable excitation, binding energy and simple preparation[32]. Additionally, copper oxide (CuO), a common p-type semiconductor with a low band gap energy, is also antibacterial, anti-inflammatory and has excellent chemical stability[39]. ZnO has been coupled with low-bandgap p-type semiconductors to demonstrate a number of properties including (i) the creation of narrow bandgap that improves visible light harvesting[34]. (ii) the development of a p-n heterojunction, which reduces the rate of e-/h+ recombination[49] and (iii) enhanced reusability without sacrificing substantial performance[35]. To obtain these features, CuO/ZnOnano structured materials must be developed.

For the fabrication of CuO/ZnO nanocomposite, synthetic approaches such as wet impregnation, sol-gel method, chemical vapour deposition, microwave irradiation, co-precipitation and mechanical alloying methods[2] were employed which are not cost-effective and detrimental to the environment. As a result, researchers have devised an alternative strategy for the synthesis of CuO/ZnO nanocomposite using green technologies which are favored as they are more environmentally friendly, cost-effective and can be easily scaled up with increased stability and morphology[3]. CuO/ZnO nanocomposite made using environmentally friendly methods has a distinctive shape and has effective particle size reduction which increases the production of reactive oxygen species (ROS) in photocatalysis and antibacterial activity.

One of the most important resources for human survival is fresh water. Dye-infused wastewater has a significant negative impact on both the environment and human health. It typically goes off from the industries that produce plastics, textiles, papers and leather[31]. Some of the methods that have

been developed for dye removal include precipitation, ion exchange, adsorption, photodegradation and biodegradation[1]. Photodegradation of dyes can be used for treatment of waste water tainted with dyes.

Methylene blue (MB) is one of the dyes that is most frequently used in the textile industry. These colors must be broken down first to prevent pollution of the water. This mechanism involves charge transfer and separation which can be facilitated by heterostruture[21,30]. Hierarchical metal oxide nanoparticles such as CuO/ZnO can be employed as an extremely effective photocatalyst for MB degradation[15,18,50].

Here, we present a general, ecofriendly *Cimpobogan citrates* (lemon grass) leaf extract that was employed to synthesise CuO/ZnO nanocomposite in a way that was environmentally friendly for capping, stabilizing and reducing agent. The leaf of Cimpobogan citrates has phytochemical components of flavonoids, carbohydrates, tannins, alkaloids, steroids and phytosteroids all existing in leaves[26]. The photocatalytic activity of *Cimpobogan citrates* produced nanocomposite was utilized to assess the photodegradation efficiency of methylene blue (MB) dye. The importance of photocatalysts lies on the fact that they can be used with minimal supervision. Since they are heterogenous catalysts, they can be removed from water by simple filtration techniques. The reduction of bandgap due to the formation of nanocomposites makes them operable in the presence of sunlight.

The nanocomposites expose a maximum surface area which can be utilized for the effective adsorption of molecules for photocatalysis. Additionally, the antibacterial activity of two bacterial strains, *Escherichia coli* and *Staphylococcus aureus*, was tested using the agar disc diffusion method. The antibacterial activity of the nanocomposites can also be beneficial in decontamination of microorganisms in water. These properties of nanocomposites make an effective argument for their use. Prepared nanocomposites were characterized using UV-Vis, FT-IR, XRD, SEM with EDAX and HR-TEM.

Material and Methods

Chemicals and Reagents: *Cimpobogan citrates* (leaves) were obtained near Sri Paramakalyani College, Alwarkurichi, Tamil Nadu, India. Analytical grade copper sulfate pentahydrate ($CuSO_4.5H_2O$, 99 %), zinc acetate dihydrate [$Zn(CH_3COO)_2.2H_2O$, 99%], methylene blue ($C_{16}H_{18}ClN_3S$) and ethanol were purchased from Sigma Aldrich, Bangalore, India. Throughout the experiment, deionized water (DW) was used for washing and solution preparation.

Extract Preparation: The *Cimpobogan citrates* plant's leaves were gathered and cleaned in distilled water, allowed to dry by air and then processed into a powder using a grinder. After that, in a 500 ml beaker, containing 5 g of CC powder and 150 ml of DW were combined and the mixture was allowed to react under magnetic stirring for 10 min. The extract was filtered after cooling and kept at 4 °C for use in upcoming investigations. The schematic diagram is shown in scheme 1.

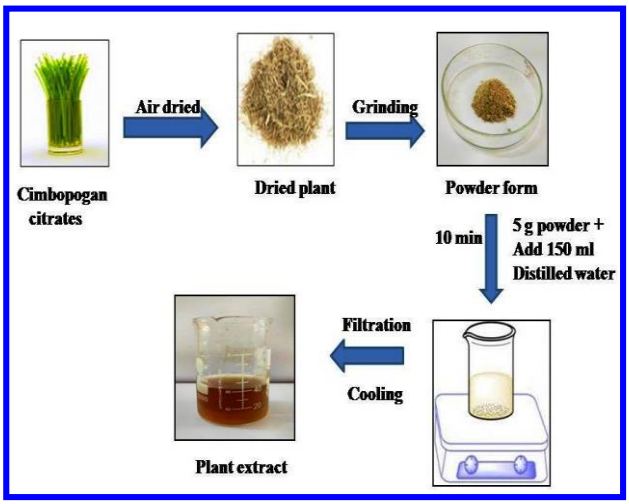

Scheme 1: Schematic diagram of extract from *Cimpobogan citrates* plant

Preparation of ZnONPs: 4 g of zinc (II) acetate was dissolved in 70 ml of distilled water and add 30 ml CC extract solution. At room temperature, the mixture was stirred for 30 minutes. The solution was put into a 100 mL teflon-coated autoclave and heated to 180 °C for six hours in a Muffle furnace. Then dark solution was centrifuged for 10 minutes at 6000 rpm to obtain ZnONPs and it was washed several times using H_2O and C_2H_5OH mixture and then it was dried at 60 °C for 12 hrs.

Preparation of CuONPs: CuONPs was obtained by using 4 g copper (II) sulphate (CuSO4. 5H2O) dissolved in water (70 ml) and 30 ml of CC extract and then stirred for 30 min. to create a homogeneous solution. It was put into a 100 ml Teflon autoclave and heated to 180 °C for six hours. A dark brown precipitate was obtained which was collected by centrifuge method and the impurity was removed by using H_2O and C_2H_5OH mixture. The precipitate was dried at 80^o C for 12hrs to get CuONPs powder.

Synthesis of CuO/ZnO Nanocomposite: ZnO/CuO nanocomposite was synthesised environmentally friendly using *Cimpobogan citrates* leaf extract and the hydrothermal technique. In this procedure, a solution with a volume ratio of 40 ml of the extract and 40 ml of DW was dissolved with 3 g of copper (II) sulphate and 1 g of zinc (II) acetate. For an hour, the aforementioned components were mixed thoroughly. The mixes were then transferred to a teflon-lined autoclave and heated to 180°C for three hours. Centrifugation at 6000 rpm for 10 minutes separated the resulting light brown precipitate from the reaction suspension. It was then continuously washed with H_2O and C_2H_5OH and dried in for six hours at 80 °C. The schematic diagram synthesis of ZnO/CuO nanocomposite is shown in scheme 2.

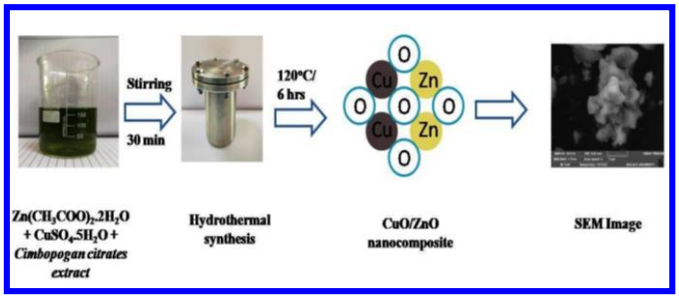

Scheme 2: Schematic illustration of preparation of CuO/ZnO nanocomposite by using hydrothermal method

Instrumentation and experimental methods: For all the nanocomposites, FT-IR spectra (Nicolet IS5R FTIR, KBR windows with AR Diamond crystal plate, Make: Thermofisher) were taken in order to identify the functional groups. With water being used as a reference, the absorption spectra were captured using a UV-Visible spectrophotometer (Hitachi UH-5300 spectrophotometer Double beam). Crystalinity and phase purity of X-ray diffractometers (Bruker Eco D8 Advance) were investigated. The nanoparticles' shape and elemental composition were examined using SEM and EDAX (vega 3 Tescan). Using HR-TEM (Jeol, JEM 2100), the NPs' morphology was evaluated.

The photo catalytic degradation study: ZnONPs, CuONPs and CuO/ZnO nanocomposite were prepared and tested in a cylindrical quartz tube photoreactor. A 365 nm visible light lamp (250 W Xenon lamp with 400 $mWcm^{-2}$ intensity) was used for irradiation. 100 ml of methylene blue (MB) dye was mixed with 100 mg of photocatalyst made of ZnONPs, CuONPs and CuO/ZnO nanocomposite at a concentration of 10 ppm (parts per million) and a visible light bulb was placed within a quartz glass tube.

The experiment was carried out at room temperature under visible light illumination after the solution was stirred for 30 min in the dark to achieve MB absorption-desorption equilibrium on the surface of ZnONPs, CuONPs and CuO/ZnO nanocomposite photocatalysts. For a maximum of 15 minute intervals, 10 ml of the MB degrading solution was collected and filtered using a 0.45 M syringe filter to remove the photocatalysts. The percentage degradation efficiency of MB was estimated using the following equation while the degradation reaction was being constantly monitored by a UV-visible spectrometer at 663 nm[29].

$$D\ (\%) = C_0\text{-}C_t/C_0 \times 100 \quad (1)$$

where C_0 and C_t represent the MB dye solution's initial and final concentrations over time respectively.

Anti-bacterial evaluation: The experiment's tools were placed in an autoclave for 20 minutes at 121 °C. *Escherichia coli* (*E.coli*) and *Staphylococcus aureus (S.aureus)* strains were grown in 50 ml of NB and incubated at 37 °C overnight before being used. The antibacterial activity of synthesised ZnONPS, CuONPs and ZnO/CuO nanocomposite was examined using the disc diffusion method. This method involved pouring 120 ml of bacterial culture onto sterile Petri plates and spreading it around with a spreader after 20 ml of sterilised Mueller Hinton agar was added.

ZnONPs, CuONPs and ZnO/CuO nanocomposite were placed onto a 6 mm sterile disc. The loaded disc was positioned on the surface of the medium and the extract was given five minutes to diffuse before the plates underwent a 24-hour incubation period at 37 °C. *Escherichia coli* (*E.coli*) and *Staphylococcus aureus (S.aureus)* bacteria were mixed with the solvents as a control[5,37]. A clear ruler was used to measure the inhibitory zones that had formed around the disc at the conclusion of the incubation period in millimeters.

Results and Discussion

UV-visible characterization: Figure 1A (a-d) shows the UV-visible spectra of CC Extract, ZnONPs, CuONPs and CuO/ZnO nanocomposite. Peaks at 230 nm, 273 nm and 320 nm appeared in the CC extract due to the presence of the phenolic compounds as shown in fig. 1A (a)[10]. A broad peak at 328 nm was obtained which was used to compare with the electronic transition of the Zn-O bond in ZnONPs as shown in fig. 1A (b). A broad peak at 253 nm and small intensity of the peak at 320 nm consistent with the Cu-O bond in CuONPs and π-π* transition of benzoyl in the extract are shown in fig. 1A (c)[46]. CuO/ZnO nanocomposite showed that a broad peak with low intensity at 334 nm was effectively coated on ZnONPs[9,14,23].

Figure 1B (a-c) shows the Tauc plot of ZnONPs, CuONPs and CuO/ZnO nanocomposite where the CuO/ZnO nanocomposite (1.56 eV) has a less band gap energy than the ZnONPs (1.69 eV) and CuONPs (1.42 eV). The low band gap energy of the CuO/ZnO nanocomposite resulted into the excellent photocatalytic degradation activity under visible light irradiation[45].

FT-IR characterization: The FT-IR spectra of CC extract, ZnONPs, CuONPs and CuO/ZnO nanocomposite is shown in fig. 2 (a-d). Figure 2(a) shows the multiple peaks at 3472 cm^{-1} (O-H stretching vibration), 3020 and 2934 cm^{-1} (C-H stretching vibration), 1738 cm^{-1} (C=O stretching vibration), 1418 cm^{-1} (-C-C- stretching vibration), 1132 cm^{-1} (C-O stretching vibration) and 763 cm^{-1} (-C-C stretching vibration) and their peaks were determined the various functional groups in CC Ext[40]. Mostly lower intensity new peaks were recorded at 2031 cm^{-1} and 946 cm^{-1} and 668 cm^{-1} and were ascribed to the C=C bond stretching, C-H bond bending vibration and Zn-O bond stretching vibration as shown in fig. 2(b)[36].

The peaks are slightly shifted to higher wave numbers at 3058 and 2958 cm^{-1} (C-H bond in CH_3 and CH_2 groups), 2182 cm^{-1} (C=C stretching vibration), 1054 cm^{-1} (-C-H bending) and 668 cm^{-1} (Cu-O stretching vibration) and other

O-H bonds and C=O bond increase the intensity of the peaks and their peaks were promised in to the formation of CuONPs as shown in fig. 2(c)[42]. Figure 2(d) displays several less intensity peaks and one peak at a higher wave number at 691 cm^{-1} (Zn-O-Cu bond stretching vibration) compared with figure 2(a) CC Ext. which witnessed the ZnONPs coated on CuONPs in ZnO/CuO nanocomposite[6,44].

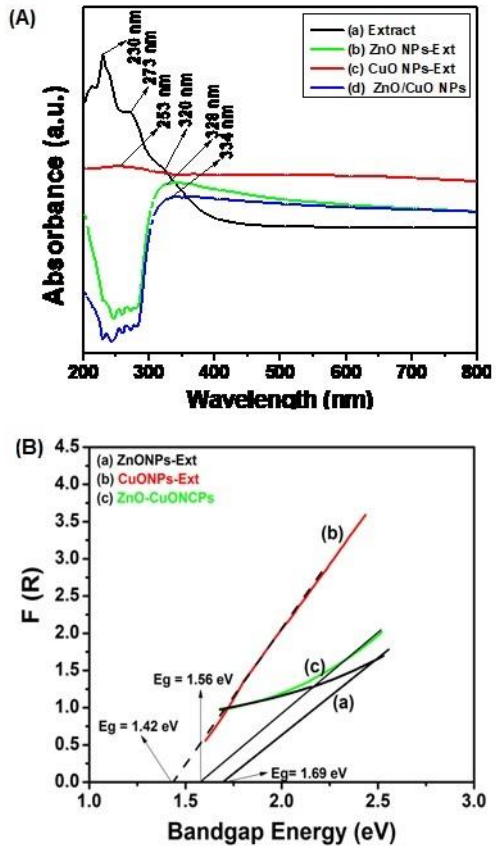

Figure 1 (A and B): (A) UV-visible absorption spectra of (a) CC extract, (b) ZnONPs, (c) CuONPs and (d) CuO/ZnO nanocompsoite and (B) Tau's Plot of (a) ZnONPs, (b) CuONPs and (c) CuO/ZnO nanocomposite.

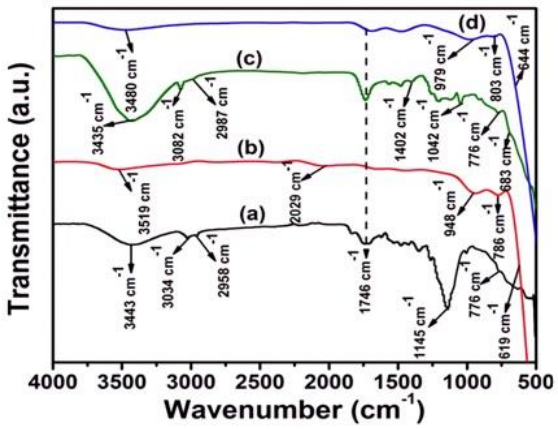

Figure 2(a-d): FT-IR spectra of (a) CC Extract, (b) ZnONPs, (c) CuONPs and (d) CuO/ZnO nanocomposite

XRD characterization: X-ray diffraction (XRD) method is used to identify the crystalinity of nanomaterials. X-ray diffraction patterns of CC extract, ZnONPs, CuONPs and CuO/ZnO nanocomposite are shown in fig. 3 (a-d). The peaks of 2θ at 22.10° (100), 30.09° (002) and 41.79° (101) were fitted to the (JCPDS#-03-0289) and (JCPDS#22-1069) which indicated the formation of a crystal plane and amorphous nature of CC extract powder as depicted in fig. 3(a)[33]. Figure 3(b) shows the diffraction peak of ZnONPs at 31.49° (100), 34.45° (002), 36.19° (101), 47.27° (102), 56.48° (110), 59.15° (103), 62.73° (200), 67.4° (112) and 68.98° (201) corresponding to a hexagonal phase of ZnO (JCPDS#00-0360-1451) while peaks at 33.36° (110), 35.38° (002), 38.52° (111), 48.67° (-202), 52.43° (020), 57.75° (202), 61.48° (-113), 66.18° (311), 67.89° (113), 71.81° (-311) and 75.20° (222) were marked as monoclinic of CuONPs (JCPDS#00-048-1548) as shown in fig. 3(c).

The CuO/ZnO nanocomposite diffraction patterns were related to the peak of ZnO NPs at 2θ values of 33.20°, 34.53°, 36.29°, 49.41°, 47.58°, 55.84°, 59.30°, 62.4° and 69.09° respectively and the remaining peaks at 2θ of 35.73°, 42.05°, 50.08°, 54.24°, 56.64°, 58.60°, 60.93°, 66.69°, 71.25° and 73.38° matched to CuONPs[4,43]. Figure 3 (d) shows high-intensity peaks due to Zn-O-Cu bond formation with the crystal of CuO/ZnO nanocomposite. The average size of ZnONPs, CuONPs and CuO/ZnO nanocomposite were calculated by using Debye Scherrer's equation.

$$D = K\lambda/\beta \cos\theta \qquad (2)$$

where D is the diameter of nanoparticles, K (0.9) is the constant, λ is the wavelength of X-ray, β is the FWHM at maximum intensity peak at θ is the Bragg angle[19,41]. The average sizes of ZnONPs-Ext and CuONPs-Ext crystallite sizes are 20 nm and 25 nm respectively.

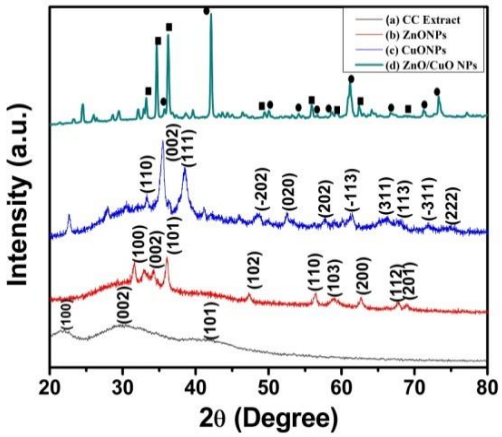

Figure 3(a-d): XRD diffraction patterns of (a) CC extract, (b) ZnONPs, (c) CuONPs and (d) CuO/ZnO nanocomposite.

Scanning Electron Microscope (SEM) characterization: Figure 4(A-D) shows the surface morphology of ZnONPs. An aggregate with sphere like structures at 10 µM is shown

in fig. 4 (A). Figure 4(B) shows compact particles obtained at high magnification 5 µM. Sphere like structures was clearly captured at the highest magnification 2 µM as shown in fig. 4(C). Energy dispersive x-ray analysis (EDAX) confirmed the existence of C, Zn and O in ZnONPs as shown in fig. 4 (D).

Figures 5(A-C) reveal the surface morphology of CuONPs at various magnification 10 µM, 5 µM and 2 µM. The aggregated particles appeared at 10 µM as illustrated in fig. 5 (A). Figure 5(B) explored that white particles were observed at 5 µM.

The brightness of the particles was visualized at high magnification 2 µM as shown in Fig.5(C). EDAX shows that the elements of C, Cu and O were stabilized in CuONPs as shown in fig. 5 (D). The various images of CuO/ZnO nanocomposite recorded at 10 µM, 5µM, 2µM and 1 µM are shown in fig. 6(A-D). Different shapes of ZnONPs coated with CuONPs are shown in fig. 6A at low magnification 10 µM. Mixture of various forms of ZnONPs with white particles of CuO NPs was taken at 5 µM as shown in fig. 6(B). Figure 6(C) shows white particles coated with ZnO NPs exposed at 2 µM. White particles of CuONPs with rod and hexagonal shape of ZnO NPs were clearly obtained at high 1 µM as shown in fig. 6 (D). EDAX of Cu, Zn and O was presented in CuO/ZnO nanocomposite as shown in fig. 6 (E).

Transmission Electron Microscope: Transmission electron microscope was used to evaluate the material's size and shape. The TEM images of CuO/ZnO nanocomposite agglomerated spherical particles were observed at 50nm and 20 nm as shown in fig. 7 (A and B). The maximum spherical shape of particles was recorded at high magnification (10 nm) as shown in fig. 7(C). At the highest magnification of 5 nm, the spherical shape of particles was clearly displayed as shown in fig. 7 (D). The SAED pattern has also confirmed the crystallinity of CuO/ZnO nanocomposite as shown in fig. 7 (E).

Photocatalytic degradation application: The photocatalytic degradation of MB was determined using different photocatalysts such as ZnONPs, CuONPs and CuO/ZnO nanocomposite with visible light illumination at different time intervals as shown in fig. 8 (A-C). The photocatalyst of ZnONPs, CuONPs and CuO/ZnO nanocomposite first absorbed the MB dye solution under dark condition. ZnONPs were demonstrated that the photocatalyst for the degradation of MB under visible light irradiation from 0 to 60 min and its peak intensity was not completely degraded as shown in figure 8(A). CuONPs almost efficiently decompose MB dye under visible light with different time range intervals from 0 to 60 min as shown in fig. 8(B). The superior photocatalytic degradation of MB was performed by CuO/ZnO nanocomposite under visible light irradiation from 0 to 60 min as shown in fig. 8(C).

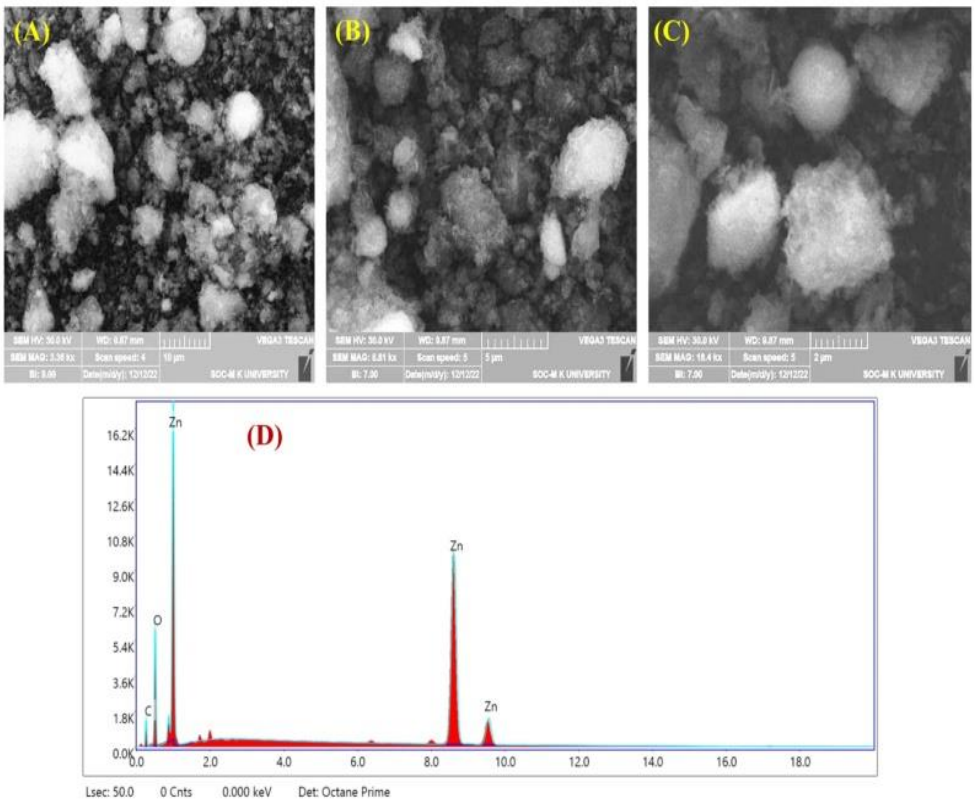

Figure 4(A-D): SEM image of ZnONPs (A) 10 µM, (B) 5 µM and (C) 2 µM and (D) EDAX elemental analysis of zinc (Zn), oxygen (O) and carbon (C)

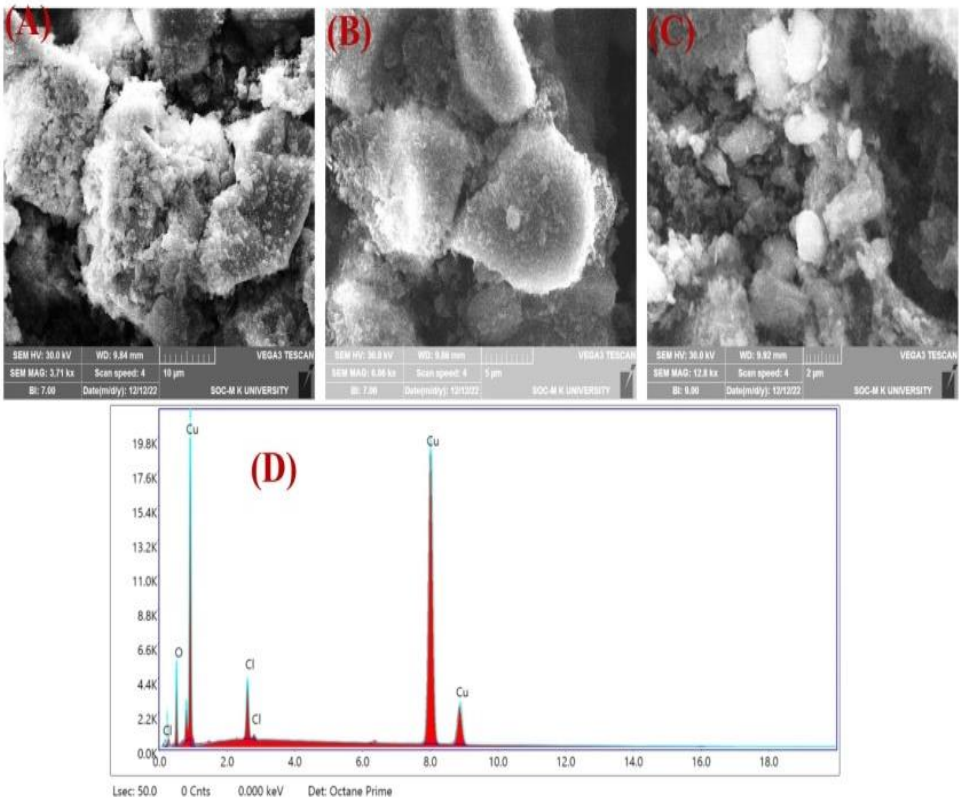

Figure 5(A-D): SEM image of CuONPs (A) 10 µM, (B) 5 µM and (C) 2 µM and (D) EDAX elemental analysis of copper (Cu), oxygen (O) and carbon (C).

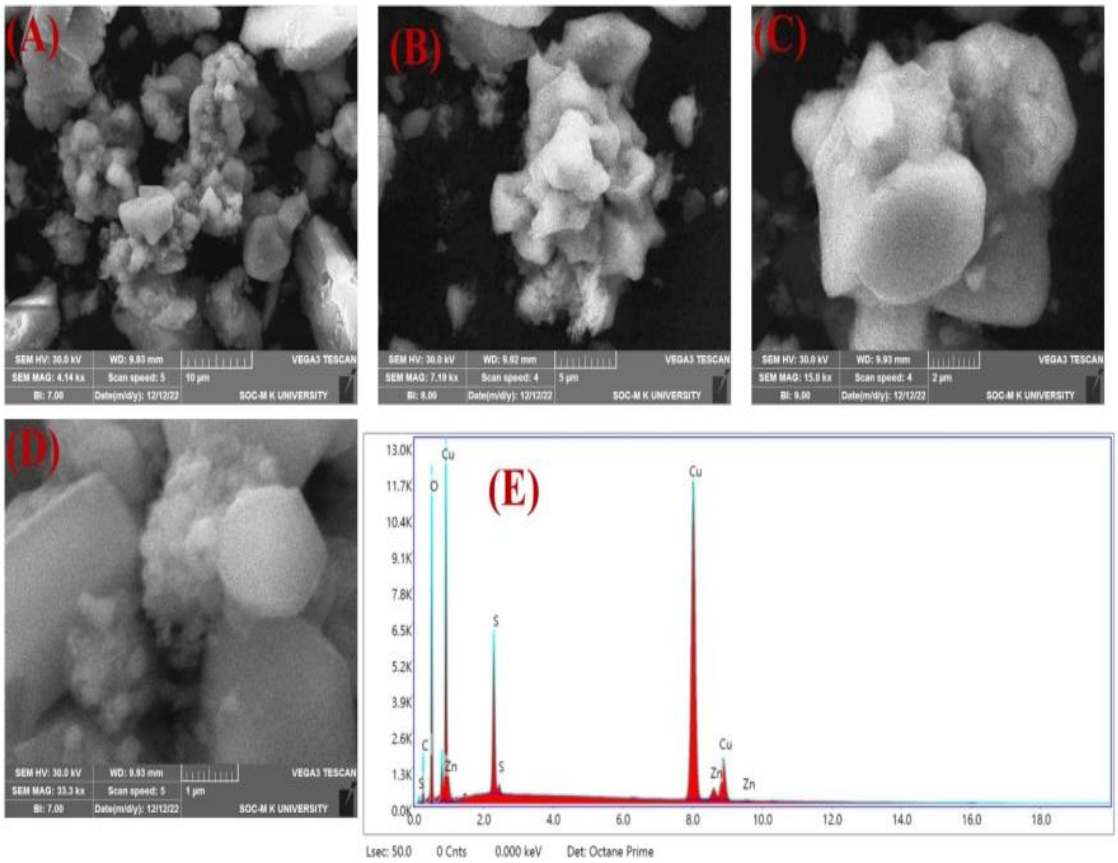

Figure 6(A-E): SEM image of CuO/ZnO NPs (A) 10 µM, (B) 5 µM and (C) 2 µM and (D) 1 µM (E) EDAX elemental analysis of zinc (Zn), copper (Cu) oxygen (O) and carbon (C)

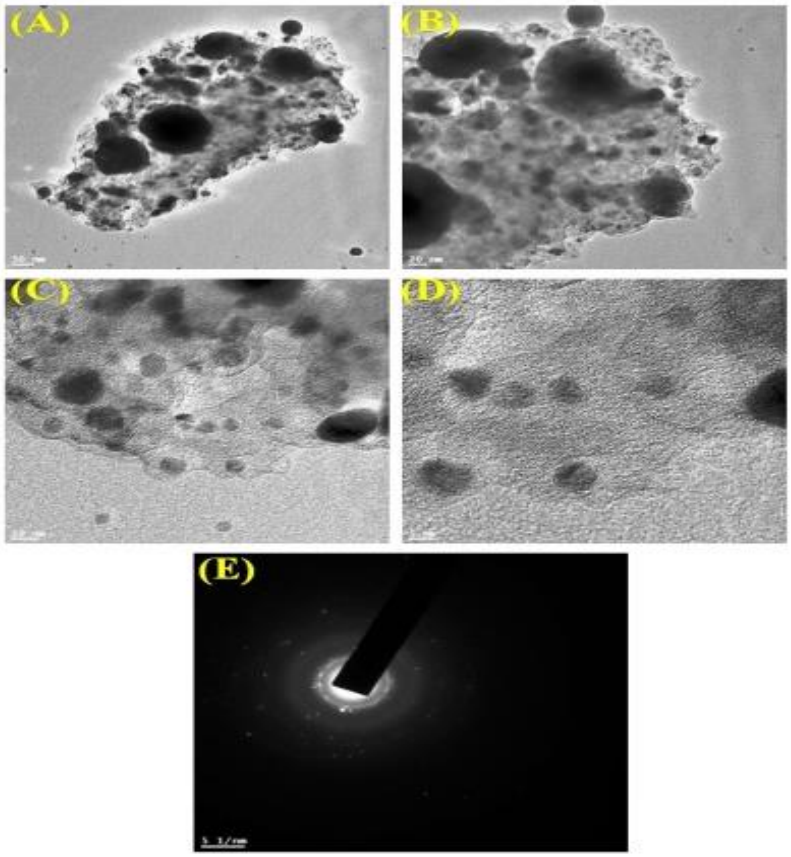

Figure 7(A-E): TEM images of the CuO/ZnO nanocomposite (A) 50 nm, (B) 20 nm, (C) 10 nm and (D) 5 nm (E) SAED pattern of CuO/ZnO nancomposite

Among them CuO/ZnO nanocomposite showed higher percentage degradation of MB than CuONPs and ZnONPs as shown in fig. 9A (a-c). Percentage degradation was calculated by using equation (1). CuO/ZnO nanocomposite demonstrated a higher photocatalytic activity due to CuONPs strongly coated on ZnONPs with lower band gap energy. The decompose kinetics rate constant of MB dye with various photocatalysts of ZnONPs, CuONPs and CuO/ZnO nanocomposite was evaluated by using the first – order rate equation[28].

$$\ln(C_t/C_0) = -kt \quad (3)$$

where C_0 and C_t are the initial and final concentrations at 0 min and time t respectively, Kinetic rate constant (K, min^{-1}) was calculated from the slope of the plot $\ln(C_t/C_0)$ vs time t as shown in fig. 9B (a-c). The larger rate constant of CuO/ZnO NCs (K= 0.0265 min^{-1}) is shown in fig. 9B (a-c).

Photocatalytic degradation mechanism of MB with ZnO-CuO nanocomposite: Figure 10 shows the photocatalytic degradation mechanism of MB with CuO/ZnO nanocomposite under visible light illumination. This nanocomposite photocatalyst is electron (e^-) and holes (h^+) generated in the conduction band (CB) and the valence band (VB). The electrons in CB band of CuO (E_g =1.46 eV) were pushed to the CB band of ZnO (Eg= 2.04 eV) whereas the holes were moved from the VB of ZnO to the VB band of CuO. The CB band of electrons in ZnO reacts with reactive oxygen species to form superoxide radicals ($\cdot O^{2-}$) and VB band of holes in CuO generates the hydroxide radicals ($^{-}OH\cdot$) after reacting with H_2O. These radicals are highly reactive species and unstable, effectively degrading MB into by products like H_2O, CO_2 and NO_3 and SO_4^{2-} etc.[11] The reaction process is as follow:

$$CuO\text{-}ZnO + h\nu \rightarrow ZnO\ (e^-_{CB} + h^+_{VB}) + CuO\ (e^-_{CB} + h^+_{VB}) \quad (4)$$
$$ZnO\ e^-(CB) + O_2 \rightarrow {}^{\bullet}O_2^- \quad (5)$$
$$CuO\ h^+(VB) + OH^- \rightarrow \bullet OH \quad (6)$$
$$\bullet O_2^- + MB \rightarrow \text{degraded products} + H_2O + CO_2 + \text{Minerals} \quad (7)$$
$$\bullet OH + MB \rightarrow \text{degraded products} + H_2O + CO_2 + \text{Minerals} \quad (8)$$
$$h^+(VB) + MB \rightarrow \text{degradation products} + H_2O + CO_2 + \text{Minerals} \quad (9)$$

Anti-bacterial activity of the samples: CuONPs, ZnONPs and CuO/ZnO nanocomposite samples were tested for the anti-bacterial activity against *Escherichia coli (E.coli*) and *Staphylococcus aureus (S.aureus)* bacteria by disc diffusion method. The antibacterial activities in presence of 120 µg/mL of the samples were shown in fig. 11 (A-D).

As noted, The CuONPs and ZnONPs samples displayed less anti-bacterial activity against both *Escherichia coli* (*E.coli*) and *Staphylococcus aureus (S.aureus)* bacteria (with zone of 20 mm of CuONPs and 12 mm of ZnONPs for *S.aureus* and 12 mm of CuONPs and 30 mm of ZnONPs for *E. coli).*

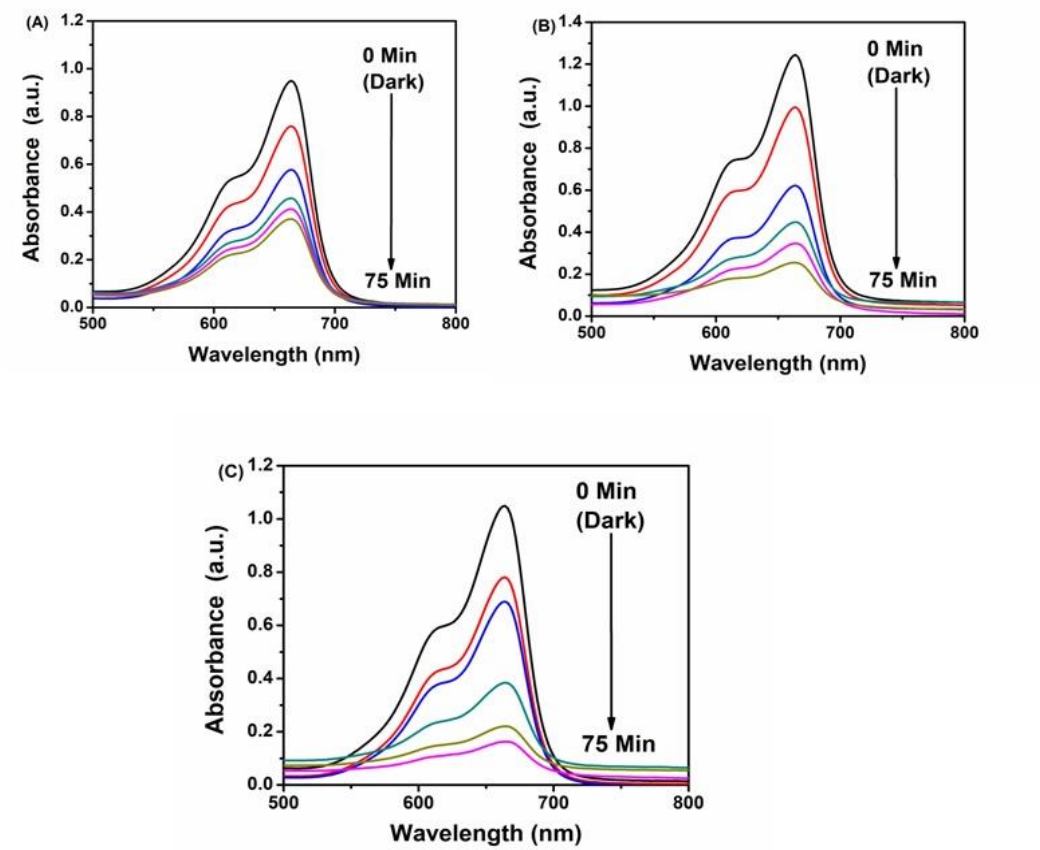

Figure 8 (A-C): Photocatalytic degradation spectra of MB using (A) ZnONPs, (B) CuONPs and (C) CuO/ZnO nanocomposite at various time interval 0 to 75 min

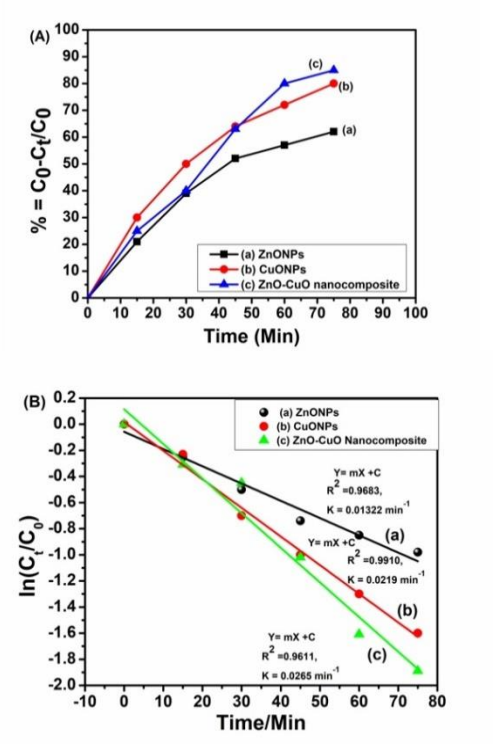

Figure 9 (A and B): (A) Percentage degradation efficiency *vs* reaction time (min) and (B) Kinetic plot of ln(C_t/C_0) *vs* reaction time (min) for MB degradation using (a) ZnONPs, (b) CuONPs(b)and (c) CuO/ZnO nanocomposite.

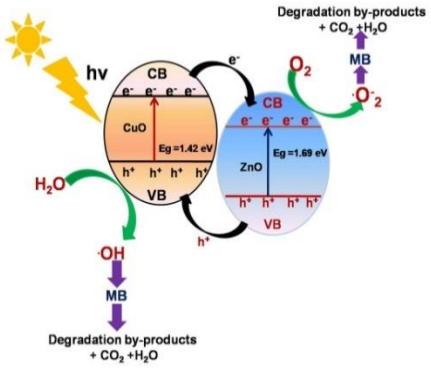

Figure 10: The photocatalytic degradation mechanism of MB with CuO/ZnO nanocomposite under visible light irradiation

However, CuONPs and ZnONPs were prepared by using *Cimbopogan citratus* extract to reduce antibacterial activity. Interestingly, CuO/ZnO nanocomposite was exhibited the higher anti-bacterial activities against both the zones of *E.coli* for 31 mm and *S.aureus* for 22 mm bacteria as shown in fig. 11 (C and D).

Conclusion

Green synthesis of CuO/ZnO nanocomposite was effectively prepared by using *Cimbopogan citrates* (CC) with the hydrothermal method. It was applied for the photocatalytic decompose of MB under visible light illuminate. FT-IR spectra confirmed the formation of Zn-O and Cu-O bonds in

the CuO/ZnO nanocomposite. Tau's plot displayed that CuO/ZnO nanocomposite has lower band gap energy (E_g = 1.46 eV). SEM image clearly indicated that the CuO particles coated on ZnO. TEM result showed that ZnO/CuO nanocomposite was slightly agglomerated in spherical shape with size around 20–50 nm.

The effective degradation of MB with CuO/ZnO nanocomposite responded better to under visible light irradiation at 85 % in 75 min. Furthermore, the ZnO/CuO nanocomposite exhibited successful antibacterial action adjacent to both gram-positive and gram-negative bacteria. Consequently, it is projected that the CC extract ZnO/CuO nanocomposite can perform as competent nanomaterials for sustainable biological and photocatalytic applications.

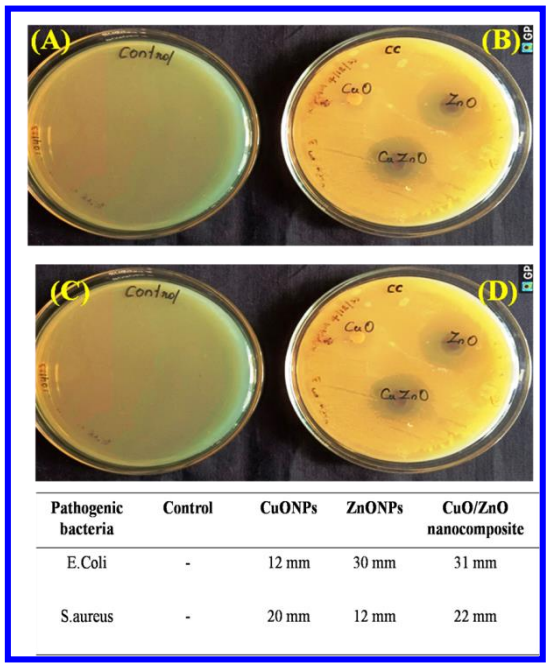

Pathogenic bacteria	Control	CuONPs	ZnONPs	CuO/ZnO nanocomposite
E.Coli	-	12 mm	30 mm	31 mm
S.aureus	-	20 mm	12 mm	22 mm

Figure 11(A-D): Anti-bacterial activities of the CuONPs, ZnONPs, CuO/ZnO nanocomposite samples against *E. coli* and *S. aureus* and (E) Comparison Result

Acknowledgement

We thank DST-FIST, India for the IR and UV instrumental facilities at the PG and Research Centre, Department of Chemistry, Sri Paramakalyani College, Alwarkurichi. The corresponding author is very much thankful to TNSCST Student project scheme. We also thank Dr. G. Ramanathan, Deparment of Microbiology, Sri Paramakalyani College for antibacterial studies.

References

1. Alam U., Fleisch M., Kretschmer I., Bahnemann D. and Muneer M., One-step hydrothermal synthesis of Bi-TiO2 nanotube/graphene composites: an efficient photocatalyst for spectacular degradation of organic pollutants under visible light irradiation, *Appl. Catal. B*, **218**, 758–769 **(2017)**

2. Alexis L., Sivasamy R., Mosquera E. and Morel M.J., High proportion ZnO/CuO nanocomposites: synthesis, structural and optical properties and their photocatalytic behavior, *Surf. Interfaces*, **17**, 100367 **(2019)**

3. Alshehri A.A. and Malik M.A., Phytomediated photo-induced green synthesis of silver nanoparticles using Matricaria chamomilla L. and its catalytic activity against Rhodamine B, *Biomolecules*, **10**, 1604 **(2020)**

4. Bekru A.G., Tufa L.T., Zelekew O.A., Goddati M., Lee J. and Sabir F.K., Synthesis of a CuO−ZnO Nanocomposite for Efficient Photodegradation of Methylene Blue and Reduction of 4-Nitrophenol, *ACS Omega*, **7**, 30908−30919 **(2022)**

5. Bhuvaneswari P., Shanmugavadivu T., Sabeena G., Annadurai G. and Sindhuja E., Synthesis and characterization of chitoson with silica (CS) nanocomposite with enhanced antibacterial activity, *Int. J. Res. Pharm. Sci.*, **13(1)**, 1-8 **(2022)**

6. Bordbara M., Negahdara N. and Nasrollahzadeh M., Melissa Officinalis L. leaf extract assisted green synthesis of CuO/ZnO nanocomposite for the reduction of 4-nitrophenol and Rhodamine B, *Separation and Purification Technology*, **191**, 295–300 **(2018)**

7. Dorneanu P.P., Airinei A., Olaru N., Homocianu M., Nica V. and Doroftei F., Preparation and characterization of NiO, ZnO and NiO–ZnO composite nanofibers by electrospinning method, *Mater. Chem. Phys.*, **148**, 1029–1035 **(2014)**

8. Dozzi M.V., Marzorati S., Longhi M., Coduri M., Artiglia L. and Selli E., Photocatalyticactivity of TiO2–WO3 mixed oxides in relation to electron transfer efficiency, *Appl. Catal. B*, **186**, 157–165 **(2016)**

9. Elumalai K., Velmurugan S., Ravi S., Kathiravan V. and Ashokkumar S., Green synthesis of zinc oxide nanoparticles using *Moringa oleifera* leaf extract and evaluation of its antimicrobial activity, *Elsevier* **134**, 158–164 **(2015)**

10. Fernandes S.C.M., Sadocco P., Alonso-Varona A., Palomares T., Eceiza A., Silvestre A.J.D., Mondragon T. and Freire C.S.R., Bioinspired antimicrobial and biocompatible bacterial cellulose membranes obtained by surface functionalization with aminoalkyl groups, *ACS Appl Mater Interfaces*, **5**, 3290–3297 **(2013)**

11. Harish S., Archana J., Sabarinathan M., Navaneethan M., Nisha K.D., Ponnusamy S., Muthamizhchelvan C., Ikeda H., Aswal D.K. and Hayakawa Y., Controlled structural and compositional characteristic of visible light active ZnO/CuO photocatalyst for the degradation of organic pollutant, *Appl. Surf. Sci.*, **418**, 103–112 **(2017)**

12. Hassanpour M., Hojaghan H.S. and Niasari M.S., Degradation of methylene blue and Rhodamine B as water pollutants via green synthesized Co3O4/ZnO nanocomposite, *J. Mol. Liq.*, **229,** 293–299 **(2017)**

13. Hassanpour M., Salavati-Niasari M., Mousavi S.A., Safardoust-Hojaghan H. and Hamadanian M., CeO2/ZnO Ceramic nanocomposites, synthesized via microwavemethod and used for decolorization of dye, *J. Nanostruct.*, **8(1)**, 97–106 **(2018)**

14. Islam M.T., Dominguez A., Alvarado-Tenorio B., Bernal R.A., Montes M.O. and Noveron J.C., Sucrose-Mediated Fast

Synthesis of Zinc Oxide Nanoparticles for the Photocatalytic Degradation of Organic Pollutants in Water, *ACS Omega*, **4**, 6560−6572 **(2019)**

15. Joshi S., Ram kumar C.B., Jones L., Mayes E.L.H., Ippolito S.J. and Sunkara M.V., Modulating interleaved ZnO assembly with CuO nanoleaves for multifunctional performance: perdurable CO_2 gas sensor and visible light catalyst, *Inorganic Chemistry Frontiers*, **4**, 1848 **(2017)**

16. Juma A.O., Arbab E.A.A., Muiva C.M., Lepodise L.M. and Mola G.T., Synthesis and characterization of CuO-NiO-ZnO mixed metal oxide nanocomposite, *J. Alloys Compd.*, **723**, 866–872 **(2017)**

17. Kaviyarasu K., Maria Magdalane C., Anand K., Manikandan E. and Maaza M., Synthesis and characterization studies of MgO:CuO nanocrystals by wetchemical method, *Spectrochim. Acta Part A: Mol. Biomol. Spectrosc.*, **142**, 405–409 **(2015)**

18. Kim J.W., Porte Y., Ko K.Y., Kim H. and Myoung J.M., Micropatternable Double-Faced ZnO Nanoflowers for Flexible Gas Sensor, *ACS Applied Materials & Interfaces*, **9**, 32876 **(2017)**

19. Kirankumar V.S. and Sumathi S., A Review on Photodegradation of Organic Pollutants Using Spinel Oxide, *Mater. Today Chem.*, **18**, 100355 **(2020)**

20. Lu P., Zhou W., Li Y., Wang J. and Wu P., Abnormal room temperature ferromagnetism in CuO/ZnO nanocomposites via hydrothermal method, *Appl. Surf. Sci.*, **399**, 396–402 **(2017)**

21. Luo G., Jiang X., Li M., Shen Q., Zhang L. and Yu H., Facile Fabrication and Enhanced Photocatalytic Performance of Ag/ AgCl/rGO Heterostructure Photocatalyst, *ACS Appl. Mater. Interfaces*, **5**, 2161−2168 **(2013)**

22. Mihindukulasuriya S.D.F. and Lim L.T., Nanotechnology development in food packaging: a review, *Trends Food Sci. Technol.*, **40,** 149–167 **(2014)**

23. Mohammadi-Aloucheh R., Habibi-Yangjeh A., Bayrami A., Latifi-Navid S. and Asadi A., Green synthesis of ZnO and ZnO/CuO nanocomposites in *Mentha longifolia* leaf extract: characterization and their application as antibacterial agents, *Journal of Materials Science: Materials in Electronics*, **29**, 13596–13605 **(2018)**

24. Mousavi S.A., Hassanpour M., Niasari M.S., Hojaghan H.S. and Hamadanian M., Dy2O3-CuO nanocomposites: microwave assisted synthesis and investigated photocatalytic properties, *J. Mater. Sci. Mater. Electron*, **29**, 1238–1245 **(2018)**

25. Muller K., Bugnicourt E., Latorre M., Jorda M., Echegoyen Y.S., Lagaron J.M., Miesbauer O., Bianchin A., Hankin S., Bolz U., Perez G., Jesdinszki M., Lindner M., Scheuerer Z., Castello S. and Schmid M., Review on the processing and properties of polymer nanocomposites and nanocoatings and their applications in the packaging, automotive and solar energy fields, *Nanomaterials*, **7**, 1–74 **(2017)**

26. Naik M.M., Naik H B., Nagaraju G., Vinuth M., Vinu K. and Rashmi S.K., Effect of aluminium doping on structural, optical, photocatalytic and antibacterial activity on nickel ferrite nanoparticles by sol–gel auto-combustion method, *Journal of Materials Science: Materials in Electronics*, **29**, 20395 **(2018)**

27. Palmero P., Structural ceramic nanocomposites: a review of properties and powders' synthesis methods, *Nanomaterials*, **5**, 656–696 **(2015)**

28. Prabakaran E. and Pillay K., Self-Assembled Silver Nanoparticles Decorated on Exfoliated Graphitic Carbon Nitride/Carbon Sphere Nanocomposites as a Novel Catalyst for Catalytic Reduction of Cr(VI) to Cr(III) from Wastewater and Reuse for Photocatalytic Applications, *Acs Omega*, **6(51)**, 35221–35243 **(2021)**

29. Prabakaran E., Velempini T., Molefe M. and Pillay K., Comparative study of KF, KCl and KBr doped with graphitic carbon nitride for superior photocatalytic degradation of methylene blue under visible light, *Journal of Materials Research and Technology*, **15**, 6340-6355 **(2021)**

30. Prabhu Y.T., Rao V.N., Shankar M.V., Sreedhar B. and Pal U., The facile hydrothermal synthesis of CuO@ZnO heterojunction nanostructures for enhanced photocatalytic hydrogen evolution, *New J. Chem.*, **43**, 6794-6805 **(2019)**

31. Pu M., Guan Z., Ma Y., Wan J., Wang Y., Brusseau M.L. and Chi H., Synthesis of ironbased metal- organic framework MIL-53 as an efficient catalyst to activate persulfate for the degradation of Orange G in aqueous solution, *Appl. Catal. A*, **549**, 82–92 **(2018)**

32. Qi K., Cheng B., Yu J. and Ho W., Review on the improvement of the photocatalytic and antibacterial activities of ZnO, *J. Alloy. Compd.*, **727**, 792–820 **(2017)**

33. Saha A., Sharabani T., Evenstein E., Daniel Nessim G., Noked M. and Sharma R., Probing Electrochemical Behaviour of Lignocellulosic, Orange Peel Derived Hard Carbon as Anode for Sodium Ion Battery, *J. Electrochem. Soc.*, **167**, 090505 **(2020)**

34. Sahu K., Bisht A., Kuriakose S. and Mohapatra S., Two-Dimensional CuO-ZnO Nanohybrids with Enhanced Photocatalytic Performance for Removal of Pollutants, *J. Phys. Chem. Solids*, **137**, 109223 **(2020)**

35. Sandhya J. and Kalaiselvam S., UV Responsive Quercetin Derived and Functionalized CuO/ZnO Nanocomposite in Ameliorating Photocatalytic Degradation of Rhodamine B Dye and Enhanced Biocidal Activity against Selected Pathogenic Strains, *J. Environ. Sci. Health, Part A*, **56**, 835−848 **(2021)**

36. Sathishkumar G., Rajkuberan C., Manikandan K., Prabukumar S., DanielJohn J. and Sivarama Krishnan S., Facile biosynthesis of antimicrobial zinc oxide (ZnO) nanoflakes using leaf extract of Couroupita guianensis, *Aubl. Mater. Lett.*, **222**, 200 **(2018)**

37. Shanmugavadiv T., Bhuvaneswari P., Sabeena G., Annadurai G. and Sindhuja E., Synthesis and characterization of chitoson with monomorllonite nanocomposite (CNC) with enhanced antibacterial activity, *J. Bio. & Env. Sci.*, **21**, 148-156 **(2022)**

38. Sharma R.K. and Ghose R., Synthesis of Co3O4-ZnO mixed metal oxide nanoparticles, By homogeneous precipitation method, *J. Alloys Compd.*, **686**, 64–73 **(2016)**

39. Singh J Kaur G. and Rawat M., A brief review on synthesis and characterization of copper oxide nanoparticles and its applications, *J. Bioelectron Nanotechnol.,* **1**, 1–9 **(2016)**

39. Singh K., Singh J. and Rawat M., Green synthesis of zinc oxide nanoparticles using Punica Granatum leaf extract and its application towards photocatalytic degradation of Coomassie brilliant blue R-250 dye, *SN Appl. Sci.*, **1**, 1–8 **(2019)**

40. Soleimani E. and Taheri R., Synthesis and surface modification of CuO nanoparticles: Evaluation of dispersion and lipophilic properties, *Nano-Struct. Nano-Objects,* **10**, 167–17 **(2017)**

41. Sunday A.A., Aderonke S.F., Femi A.F. and Abel K.O., Green synthesis of copper oxide nanoparticles for biomedical application and environmental remediation, *Heliyon*, **6**, 7 **(2020)**

42. Taufique M.F.N., Haque A., Karnati P. and Ghosh K., ZnO−CuO anocomposites with Improved Photocatalytic Activity for Environmental and Energy Applications, *J. Electron. Mater*, **47**, 6731−6745 **(2018)**

43. Thatikayala1 D. and Min B., Ginkgo leaves extract-assisted synthesis of ZnO/CuO nanocrystals for efficient UV-induced photodegradation of organic dyes and antibacterial activity, *J Mater Sci: Mater Electron,* **32**, 17154-17169 **(2020)**

44. Vaiano V., Chianese L., Rizzo L. and Iervolino G., Visible light driven oxidation of arsenite to arsenate in aqueous solution using cu-doped ZnO supported on polystyrene pellets, *Catal. Today*, **361**, 69–76 **(2021)**

45. Vaiano V., Iervolino G. and Rizzo L., Cu-doped ZnO as efficient photocatalyst for the oxidation of arsenite to arsenate under visible light, *Appl. Catal. B Environ.*, **238**, 471–479 **(2018)**

46. Vidic J., Stankic S., Haque F., Ciric D., Le Goffic R., Vidy A., Jupille J. and Delmas B., Selective antibacterial effects of mixed ZnMgO nanoparticles, *J. Nanopart. Res.*, **15**, 1595 **(2013)**

47. Wang Z., Yang M., Shen G., Liu H., Chen Y. and Wang Q., Catalytic removal of benzeneover CeO2–MnOx composite oxides with rod-like morphology supporting PdO, *J. Nanopart. Res.*, **16**, 2367 **(2014)**

48. Yendrapati Taraka T.P., Gautam A., Jain S.L., Bojja S. and Pal U., Controlled Addition of Cu/Zn in Hierarchical CuO/ZnO p-n Heterojunction Photocatalyst for High Photoreduction of CO2 to MeOH, *J. CO2 Util.*, **31**, 207−214 **(2019)**

49. Zang Z., Efficiency enhancement of ZnO/Cu_2O solar cells with well oriented and micrometer grain sized Cu_2O films, *Applied Physics Letters*, **112**, 042106 **(2018)**

50. Zangeneh H., Zinatizadeh A.A.L., Habibi M., Akia M. and Isa M.H., Photocatalytic oxidation of organic dyes and pollutants in wastewater using different modified titanium dioxides: A comparative review, *J. Ind. Eng. Chem.*, **26**, 1–36 **(2015)**.

(Received 29th September 2023, accepted 30th October 2023)